Lab on a Chip

Accepted Manuscript

ROYAL SOCIETY OF CHEMISTRY

www.rsc.org/loc

Quantitative Carbon Detector (QCD) for Calibration-Free, High-Resolution Characterization of Complex Mixtures

Saurabh Maduskar[1,2,‡], Andrew R. Teixeira[1,‡], Alex D. Paulsen[1,2,‡], Christoph Krumm[1,2,‡], Trantifillios J. Mountziaris[1], Wei Fan[1], Paul J. Dauenhauer[1,2*]

[1]University of Massachusetts Amherst, Department of Chemical Engineering, 686 North Pleasant Street, 157 Goessmann Laboratory, Amherst, MA, 01003, USA.
[2]University of Minnesota, Department of Chemical Engineering and Materials Science, 432 Amundson Hall, 421 Washington Ave. SE, 55455, USA.
*Corresponding Author: hauer@umn.edu
‡Authors contributed equally.

Keywords: Microreactor, Integrated Chemistry, Fuels, Chromatography, Detector

Abstract. Current research of complex chemical systems, including biomass pyrolysis, petroleum refining, and wastewater remediation requires analysis of large analyte mixtures (>100 compounds). Quantification of each carbon-containing analyte by existing methods (flame ionization detection) requires extensive identification and calibration. In this work, we describe an integrated microreactor system called the Quantitative Carbon Detector (QCD) for use with current gas chromatography techniques for calibration-free quantitation of analyte mixtures. Combined heating, catalytic combustion, methanation and gas co-reactant mixing within a single modular reactor fully converts all analytes to methane (>99.9%) within a thermodynamic operable regime. Residence time distribution of the QCD reveals negligible loss in chromatographic resolution consistent with fine separation of complex mixtures including cellulose pyrolysis products.

1.0 Introduction. Quantification of unresolved complex mixtures (UCMs) is a major analysis obstacle in a number of emerging chemical and energy applications. For example, development of renewable, biomass-derived fuels has led to increasing complexity of liquid mixtures (10^2-10^3 compounds) as refinery feed stocks.[1,2] Similarly, measured contaminants in wastewater treatment systems are lumped into total organic carbon content as a metric for water safety.[3] Upwards of 80 wastewater contaminants from pharmaceuticals such as estrogen are difficult to remove and require regular monitoring.[4] Biodegraded crude oil, present in soils[5] and marine ecosystems,[6] contains thousands of compounds.[7] Additionally, understanding of the health effects from tobacco pyrolysates requires analysis of hundreds of potentially harmful chemicals.[8] These diverse challenges require demanding analytical techniques that utilize time-consuming calibration; the lack of a robust, fast and reliable analytical technique necessitates new technology for analysis of UCMs.

In the case of fast pyrolysis of biomass, lignocellulosic biomass is thermochemically converted to produce a liquid intermediate called 'bio-oil' which can be integrated within the existing fuel infrastructure.[9,10] Rapid thermal breakdown of lignocellulose occurs through high temperature heating, resulting in biopolymer degradation to a liquid mixture consisting of hundreds of oxygenated compounds with wide-ranging properties.[1,11] Subsequent hydroprocessing produces reduced hydrocarbons which can be economically converted to liquid fuels including gasoline, diesel or jet fuel.[12,13] Analytical quantification and identification of UCMs, such as those produced from pyrolysis and subsequent upgrading, remains a limiting research capability. Using the standard methods of gas chromatography / EI-CI mass spectrometry, characterizing this mixture requires identification and quantification of sufficient number of chemical species to close the carbon balance to >90 C%.[14,15] This analytical approach relies on the ability to identify chemical species, which must then be purchased and injected for calibration of each individual chemical.[16,17] When mixtures contain several hundred species, this methodology breaks down due to: (i) the inability to effectively identify every species, (ii) limited potential for purchasing standards, and (iii) excessive time and resources needed for routinely calibrating

hundreds of chemical vapors. For these reasons, quantification of bio-oil vapors for molecular-level study remains a significant challenge.

Previous chemical studies have demonstrated the potential of combined oxidation and methanation as a method for calibration-free carbon quantification of alkanes.[18] Further development extended this method for oxygenates and phthalates.[19,20] In this work, we develop a new design using tandem catalytic oxidation/methanation to provide calibration-free carbon quantification as a drop-in, fully-integrated microreactor. Thermodynamic calculations confirm operability at a wide range of conditions, identify fundamental detection limits, and extend the technology to a variety of analytes. Additionally, characterization of the device residence time distribution allows for optimal peak resolution for analysis of UCMs.

Utilization of an integrated microreactor (Figure 1) with additional gas flows controlled with an electronic pressure controller in a gas chromatograph allows for individual species to be converted as they exit a separating GC column by the following reactions: (a) complete oxidation (X_C>99.9%) converts organic carbon within vapors to CO_2 (Rxn. 1), and (b) the second microreactor converts all CO_2 (X_{CO2}>99.9%) to methane (Rxn. 2).

$$C_xH_yO_z + nO_2 \xrightarrow{\text{Pt on Silica/Al}_2\text{O}_3} xCO_2 + \frac{1}{2}xO_2 \qquad \text{Rxn. 1}$$

$$xCO_2 + 4xH_2 \xrightarrow{\text{Ni on Al}_2\text{O}_3} xCH_4 + 2xH_2O \qquad \text{Rxn. 2}$$

By this method, all organic vapors exiting a packed/capillary column are converted to methane before entering the GC Flame Ionization Detector (FID); FID response per mole of carbon then remains constant for all organic species. Sufficiently robust system design ensures that all possible carbonaceous species are converted to CO_2, while the integrated reactor minimizes mixing and maintains resolution necessary for analytical separation. Here, we provide experimental evidence that the QCD technique provides broad capability for carbon quantification for a wide range of species found in liquid/vapor mixtures such as bio-oil.

2.0 Experimental Methods. The QCD was designed for integration within existing gas chromatographs equipped with a capillary column and flame ionization detector (section 2.1). Feasibility of the QCD system to fully oxidize and methanate analytes (>99.9%) was shown via thermodynamic calculations (section 2.2). Residence time distribution experiments were conducted to demonstrate that the QCD technology does not interfere with chromatographic separation (section 2.3). Experiments demonstrated that the QCD output has identical carbon quantification capabilities to conventional FID-calibration methods (section 2.4). Finally, the QCD methodology was utilized in the pyrolysis of cellulose to demonstrate its capability for quantifying complex mixtures with high resolution (section 2.5).

2.1 Design and Implementation of QCD. The QCD consisted of an insulated, aluminum block (2 in. by 2 in. by 2 in.) with four cylindrical holes machined lengthwise (Figure 1). Two holes each contained a cylindrical, electrically-resistive heater (Omega Engineering PN CIR 3021, 100W), which heated the entire assembly to 500 °C. The two remaining holes housed catalytic reactor chambers comprised of 1/8” stainless steel tubing with 1/16" zero dead volume reducing union (Vici Valco PN ZRUF211) on either end. A fifth cylindrical hole was drilled to a depth of 1.0 inch at the center of the block for a thermocouple (Omega Engineering PN TC-GG-K-20-36). Temperature was controlled with an Omega CN7823 PID controller performing a feedback loop measuring the temperature within the heating block and triggering AC pulses (120 V) through a solid state relay. The first catalytic reactor chamber was utilized for catalytic oxidation. 115 milligrams of 10% Pd/Alumina (Sigma-Aldrich #440086) was packed within the first catalytic reactor chamber. Prior to entering the reactor chamber, a 1/16” zero dead volume reducing tee (Vici Valco P/N# TCEF211) combined the capillary GC column effluent with flowing oxygen (to ensure complete oxidation). Effluent from the catalytic oxidation reactor chamber was transferred to the second catalytic reactor chamber for methanation via a 1/16” stainless steel capillary transfer line. The transfer line connected to a reducing tee, which combined the effluent of the first catalytic reactor chamber with flowing hydrogen gas (to ensure complete methanation). The second catalytic reactor chamber was packed with 124 milligrams of Nickel catalyst (Agilent Technologies, P/N

5080-8761). Gases exited the second catalytic reaction chamber through a reducing union (VICI Valco PN ZRUF211) into a deactivated capillary column (8 inches long), which directed flow to the existing flame ionization detector (FID). Figure 1b includes a detailed schematic of the QCD system.

Implementation of the QCD within a gas chromatograph with an existing flame ionization detector (FID) required two supplementary gas flow lines (oxygen and hydrogen), as shown in Figure 1b. Oxygen flow was supplied to the QCD by an electronic pressure controller (EPC, Agilent PN 7890A). Excess oxygen served to ensure complete combustion of GC analytes. Total required oxygen gas flow to guarantee high yield of CO_2 (>99.9%) in the first catalytic reactor chamber of the QCD was determined by the thermodynamic calculations described in section 2.2. Implementation of oxygen flow was achieved in the experimental system by varying the oxygen set pressure and measuring the resulting oxygen flow with a bubble column. Oxygen pressure was set in all experiments to maintain oxygen flow at 1.0 sccm.

Hydrogen gas flow was controlled by the existing EPC (Agilent PN 7890A), which adjusts the hydrogen gas pressure at the inlet to the QCD. Hydrogen gas serves two purposes: (i) promotes methanation of CO_2 to CH_4, and (ii) converts excess O_2 from the combustion reactor to water. Total required hydrogen gas flow to guarantee high yield of methane (>99.9%) was determined by the thermodynamic calculations of section 2.2. Implementation of this flow was achieved in the experimental system by varying the hydrogen set pressure and measuring the resulting hydrogen flow with a bubble column. Hydrogen pressure was set in all experiments to maintain hydrogen flow at 10.0 sccm.

2.2 Calculation of Thermodynamic Microreactor Output. Thermodynamic ternary maps shown in Figure 2 were generated using a Gibbs free energy minimization method within Aspen Plus 7.3. Calculations were performed to determine the amount of supplementary hydrogen flow needed to fully methanate the carbon from the injected sample. The stoichiometry from reactions 1 and 2 was defined as a constraint on the calculations, where the injected carbon was allowed to react with supplementary oxygen and hydrogen to form CO, CO_2, CH_4, H_2O, H_2, or O_2.

$$xC + yO_2 + zH_2 \rightarrow CO + CO_2 + CH_4 + H_2O + H_2 + O_2 \qquad \text{Rxn. 3}$$

Calculations were performed at varying temperature for a fixed pressure of one atmosphere with the constraint of 99.9% conversion of carbon to methane. Property estimations were derived from the Peng-Robinson property method in ASPEN PLUS software, and all calculations were performed using the 'design specifications' function. The overall C:H:O ratios so obtained were plotted on ternary maps (Figure 2a).

Figures 2b and 2c depict the thermodynamics of Rxn. 1, 2 and 3 in the presence of helium carrier gas. ASPEN PLUS calculations were repeated to simulate a helium-to-carbon molar ratio of 10:1 at 500 °C. The helium-to-carbon ratio was chosen to replicate a common injection volume (one microliter) such that the injected moles of carbon divided by the peak width yields a 1:10 ratio with the carrier gas molar flowrate. The same calculations were performed using the same helium-to-carbon ratio for 12 different compounds which are plotted in Figure 2b and 2c.

2.3 Evaluation of QCD Residence Time Distribution. Residence time distribution (RTD) analysis was carried out to verify that the QCD does not significantly reduce chromatographic peak resolution. A tracer of methane gas was injected as a pulse and the resulting detector response was measured with an FID. Equal amount of methane gas (0.5 ml) was injected into the system for four different configurations: (i) a base case with conventional FID only, (ii) QCD reactor with no catalyst packing and no supplementary oxygen or hydrogen, (iii) QCD reactor with catalyst packing and no supplementary oxygen or hydrogen, and (iv) QCD reactor with catalyst packing and oxygen and hydrogen flows. The variance of each RTD curve was calculated and used to characterize the effect of packing and supplementary flows on GC peak resolution. Variance was calculated by first determining the exit age distribution as a function of time (Equation 1).

$$E(t) = \frac{C(t)}{\int_0^\infty C(t)dt} \quad (1)$$

The age distribution was then used to calculate the average residence time for each system configuration (Equation 2).

$$\bar{t} = \int_0^\infty tE(t)dt \quad (2)$$

Equation 1 and 2 were then used to calculate the variance of each RTD curve (Equation 3).

$$\sigma^2 = \int_0^\infty (t - \bar{t})^2 E(t)dt \quad (3)$$

2.4 Calibration and Quantification of Individual Species. Fifteen chemicals were independently injected into the gas chromatograph splitless inlet at varying concentration (2.0 to 3.0 carbon-millimole per mL solution). Both the QCD and standard Agilent FID were used in separate trials to quantify injected compounds. Fifteen compounds were selected to represent a range of sizes, chemical compositions, and functionalities including: (i) methyl furan, furfural, and levoglucosan, which are representative of compounds derived from cellulose pyrolysis, (ii) carbon dioxide and acetol, which are representative of compounds derived from hemicellulose pyrolysis, (iii) phenol, 2,6-dimethoxyphenol (DMP), and 3,4-dimethoxyacetophenone (DMAP), which are representative of compounds derived from lignin pyrolysis, and (iv) methane, ethanol, dimethyl ether (DME), propylene, p-xylene, n-heptane, and n-decane, which are representative of compounds derived from petroleum processing.

The GC inlet was maintained at 250 °C (320 °C for levoglucosan injections) and 25 psi under splitless inlet conditions. The pressure was selected to achieve a column flow of approximately 1.0 mL/min. The inlet was connected to an HP-5 column (Agilent PN 19091J-102), which connected directly to the QCD. The oven temperature was increased from 70 °C to 250 °C at a rate of 20 °C/min. Liquid samples were prepared in methanol or water to 5 wt% of the analyte with five injections ranging from 0.2-1.0 µl with an autosampler (Agilent PN 7693, Syringe PN G4513-8021). Gas samples were injected using two mass flow controllers (Brooks, PN 5850E) and a power supply with control module (Brooks, PN 0254). The concentration of analyte gas was controlled by varying the ratio of helium and analyte flow from the two controllers. The combined output from both mass flow controllers was injected into the GC inlet through a six-port switching valve (Vici Valco PN A26WT). Moles of injected compounds

quantified by GC-QCD were compared with moles of injected compounds quantified by conventional GC-FID by generating calibration curves for each compound (Supplementary Section).

2.5 Application of QCD for Cellulose Pyrolysis. To demonstrate the capability of the QCD to analyze complex mixtures, a bio-oil sample from cellulose fast pyrolysis was injected into the GC-QCD system. Bio-oil samples were collected using an ablative fast pyrolysis reactor, where product vapors were collected in a water quench, as previously described.[21] Microcrystalline cellulose (FMC Biopolymer PN Lattice NT-200) was pyrolyzed under nitrogen flow at 500 ºC. The quench was transferred to a 2 mL vial, and 1.0 µl was injected directly into the GC inlet.

3.0 Results and Discussion. The Quantitative Carbon Detector (QCD) is a modular carbon detection microreactor for direct integration with existing GC-FID systems, with a compact design that allows for installation within a GC oven. Modular design makes the catalytic reactor chambers interchangeable, allowing for additional applications such as oxygenate flame ionization detection (O-FID) to detect the moles of oxygen in a sample.[22] Characterization of the residence time distribution combined with thermodynamic calculation of regions of operability confirms the viability of the design. Response factors of conventional GC-FID and GC-QCD were compared to validate the ability of the QCD to reproduce FID results without prior calibration. Finally, a sample of bio-oil from cellulose pyrolysis was analyzed via GC-QCD to demonstrate negligible loss in chromatographic resolution of the QCD reactor with a complex mixture.

3.1 Evaluation of QCD thermodynamics. Figure 2a depicts a C-H-O ternary plot, which describes the calculated conditions under which the QCD reactions are thermodynamically favorable; for complete detection and quantification, each analyte must achieve full conversion to methane (>99.9%) within the QCD. Four black lines, each representing a different reaction temperature, envelop the region in which full conversion to methane is achieved for any given combination of molecules at given C-H-O ratios. C-H-O ratios that fall above a line are thermodynamically predicted to achieve >99.9% conversion to methane at the corresponding temperature. In addition, colored lines are drawn to indicate the stoichiometric constraints of the combustion and methanation reactions. The red ‘combustion line’

indicates a carbon-to-oxygen ratio of one-to-two, which is a requirement for complete combustion. The green 'combustion/methanation line' is drawn between points representing methane and water, indicating the overall stoichiometric requirement of the two combined reactions. The shaded region of Figure 2a represents the C-H-O ratios which satisfy both thermodynamic requirements for methane conversion and stoichiometric constraints for the QCD reactions (combustion and methanation), thereby defining a region of operability (shaded, grey).

In Figure 2b, the 500 °C boundary from Figure 2a is modified to include helium carrier gas flow with a helium-to-carbon molar ratio of 10:1, representative of common operating conditions. The addition of inert carrier gas raises the curve and reduces the region of thermodynamic operability with respect to Figure 2a. Finally, the C-H-O ratios of 12 compounds injected into the GC-QCD are plotted in Figure 2c. All 12 compounds exist within the thermodynamically possible regime under considered experimental conditions, indicating that all compounds should achieve high conversion to methane if the combined reactions of catalytic combustion and methane proceed to approach equilibrium.

Thermodynamic calculations predict that there exists a broad region of operability for the QCD across which analytes are completely converted to methane (>99.9). The results of these calculations were validated by the tests conducted to ensure complete conversion in the reactors (Supplementary Section). Additionally, the absence of catalyst deactivation within the QCD was confirmed by monitoring reactor conversion after 200 sample injections.

3.2 Effect of QCD on Peak Resolution. Design of the QCD results in negligible mixing or loss in peak resolution in comparison to a chromatogram obtained by conventional GC-FID. Figure 3 depicts the detected residence time distribution (RTD) from an injected pulse of methane for GC-FID and three different GC-QCD configurations. The conventional GC-FID system resulted in a sharp, narrow peak (black line) with variance of 18.2 x 10^4 s^2. The RTD obtained from the GC-QCD system with no catalyst (red line) resulted in a shallow, broad peak with an increased variance of 41.2 x 10^4 s^2. Introduction of catalyst into the QCD reactor (blue line) decreased the variance (27.3 x10^4 s^2), while supplementary oxygen and hydrogen flows (green line) further reduced the variance in RTD (24.3 x10^4 s^2).

RTD studies shown in Figure 3 verify that GC-QCD retains peak resolution comparable to GC-FID. Variance calculated from the GC-QCD peak is only slightly higher than that of the GC-FID system, indicating minimal loss in chromatographic separation. Small values in variance indicate a sharp, narrow peak, which makes separation of complex mixtures less time consuming. In the case of the GC-QCD reactor absent catalyst packing, the variance was more than double the variance with conventional GC-FID, likely due to increased residence time and increased axial mixing within the catalyst reactor chambers. The addition of catalyst and supplementary flows reduces gas residence time and mitigates the effects of the QCD reactor on peak resolution.

3.3 Comparison of GC-QCD and GC-FID. Figure 4 depicts parity plots comparing GC-QCD response to GC-FID response for all 15 selected compounds. Micromoles of carbon detected for both the GC-QCD and GC-FID are shown to be nearly identical for the each of the identified compounds with the exception of carbon dioxide. While carbon dioxide was not detectable with GC-FID (and normally requires a second detector such as a thermal conductivity detector, TCD), detection within the GC-QCD occurs via conversion to methane. Additionally, carbon monoxide was also quantifiable using the GC-QCD, because it was converted to carbon dioxide within the first catalytic reactor chamber and subsequently converted to methane downstream. Figure 5 condenses the data from Figure 4 into a single log-scale parity plot for comparison between chemical species. All of the data points in Figure 5 collapse to a single line, further confirming that GC-QCD is capable of duplicating the results of GC-FID without the need for individual calibration.

Response factors were determined for each chemical species for the GC-FID and GC-QCD techniques as depicted in Figure 6. Response factors were scaled using a methane internal standard to account for day-to-day variability in the FID (see Supplementary Section). GC-FID response factors for all 15 compounds are shown in Figure 6 as red bars and vary over an order of magnitude between compounds. In comparison, response factors calculated using GC-QCD are nearly constant across all 15 compounds within experimental error. As demonstrated, an identical GC-QCD response factor across a

range of gases and condensable liquids indicates that quantification of a broad range of chemical mixtures can be achieved.

3.4 Application of QCD for Complex Mixtures. Figure 7 depicts a GC-QCD chromatogram of a sample of cellulose fast pyrolysis bio-oil to demonstrate separation of a complex mixture. Separation with sufficient chromatographic resolution to resolve independent peaks was obtained within a 15 minute run. While the compounds in Figure 7 are unknown, the total amount of carbon can be rapidly quantified by integrating all peaks individually (multiple integrations) or simultaneously (a single integration), because the response factor for all compounds was the same. Similarly, the total amount of carbon in two overlapping peaks can be determined without complete separation or knowledge of peak identities. Rapid quantification of complex mixtures is also relevant in applications such as two-dimensional gas chromatography (GCxGC), where hundreds of compounds are separated, which makes the QCD an optimal detector for such applications.

4.0 Conclusions. The Quantitative Carbon Detector (QCD) is a fully-integrated, drop-in microreactor for calibration-free carbon quantification in gas chromatography. Combination of tandem catalytic oxidation and methanation converts all analyte carbon to >99.9% methane, leading to identical response factors for all separated species. Quantification of carbon eliminates the need to identify and calibrate individual compounds and provides the capability to detect and quantify both carbon monoxide and carbon dioxide. Integrated microreactor design utilized thermodynamic calculations to identify regions of operability that ensured complete conversion of all possible carbonaceous analytes to methane. Microreactor design including flows, catalyst chambers and fittings was characterized via residence time distribution to ensure minimal loss of resolution in analyte separation.

Acknowledgements. Primary financial support was provided from the Catalysis Center for Energy Innovation, a U.S. Department of Energy – Energy Frontiers Research Center (www.efrc.udel.edu) under Award DE-SC0001004. We acknowledge partial funding support from Reliance, Inc.

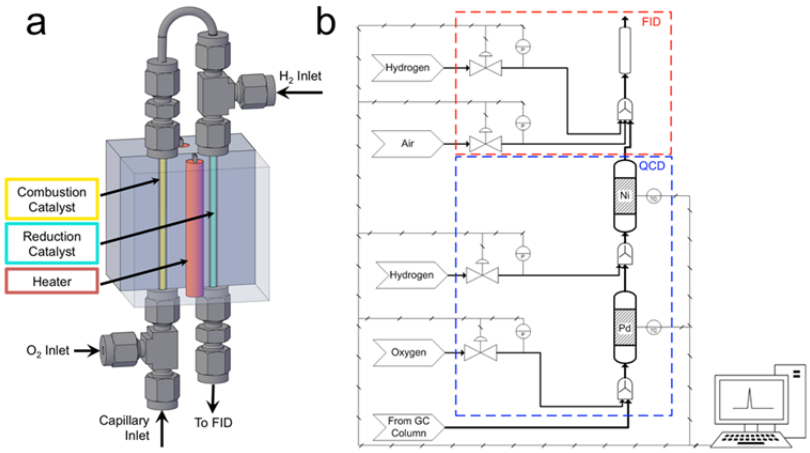

Figure 1. Design and Integration of the Quantitative Carbon Detector (QCD). a) The QCD utilizes two integrated microreactors in series for combustion and methanation to convert 99.9% of hydrocarbons to methane. b) Miniaturization of the QCD allows for drop-in integration with existing analytical tools including gas chromatography.

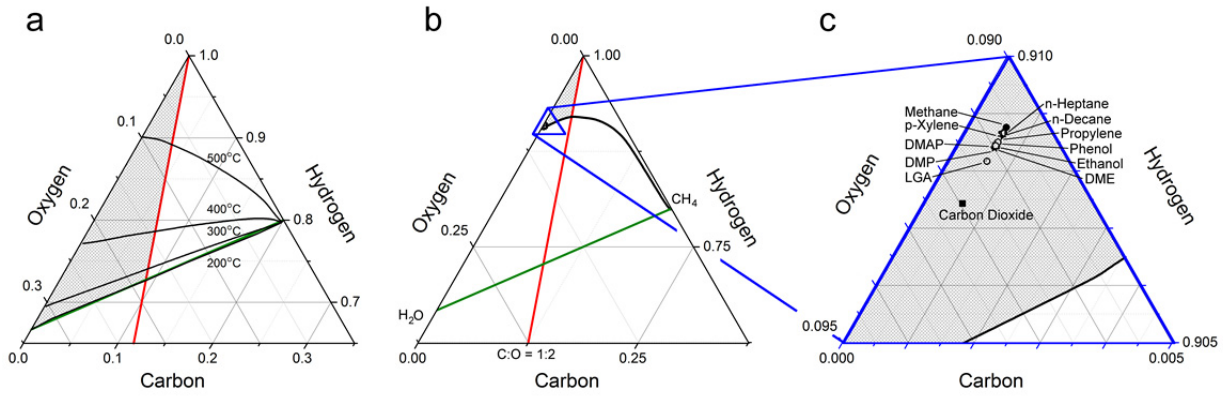

Figure 2. Thermodynamic Regimes of Operable QCD Parameters. a) Temperature dependence of thermodynamic feasibility for C:H:O ratios to achieve 99.9% conversion to methane. The shaded region envelops stoichiometric and thermodynamic bounds defining a region of QCD operability. b) At 500 °C, various compounds are plotted under dilute (He:C = 10) conditions. c) All compounds are within the operable region and are converted to methane under reaction conditions (inset).

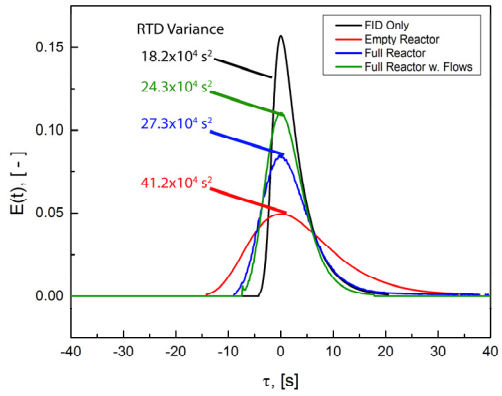

Figure 3. Residence Time Distributions in FID and QCD Detectors. RTD analysis shows minimal loss in peak resolution between GC-FID and GC-QCD. Peak resolution of the QCD is enhanced by the addition of catalyst (red versus blue) and the addition of oxygen and hydrogen flows (blue versus green).

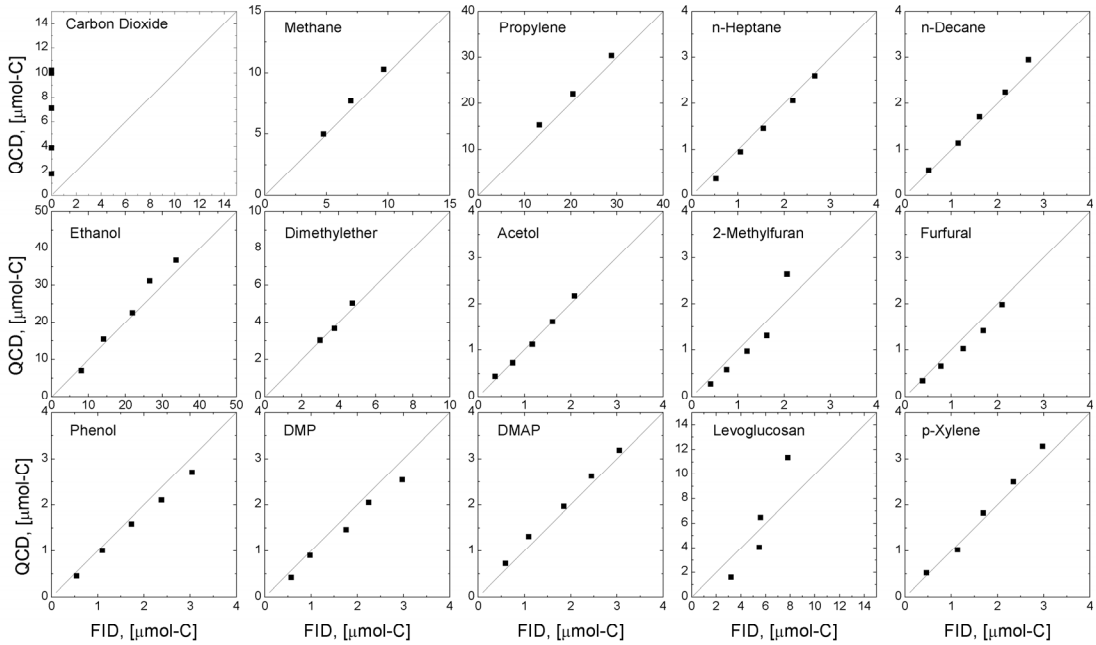

Figure 4. Individual Compound Parity of QCD and Conventional FID Quantification. Comparison of molar quantification of identical samples by both QCD and conventional, calibrated FID yield equivalent responses for a range of cellulose-, hemicellulose-, and lignin-derived pyrolysis compounds. Carbon dioxide (first panel) can only be detected by QCD (not FID).

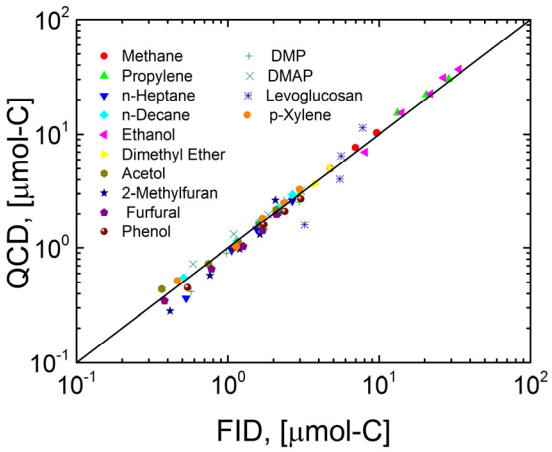

Figure 5. Collective Parity of QCD and Conventional FID Quantification. Comparison of molar quantification of identical samples by both QCD and conventional, calibrated FID yield equivalent responses for a wide range of cellulose-, hemicellulose-, and lignin-derived pyrolysis compounds.

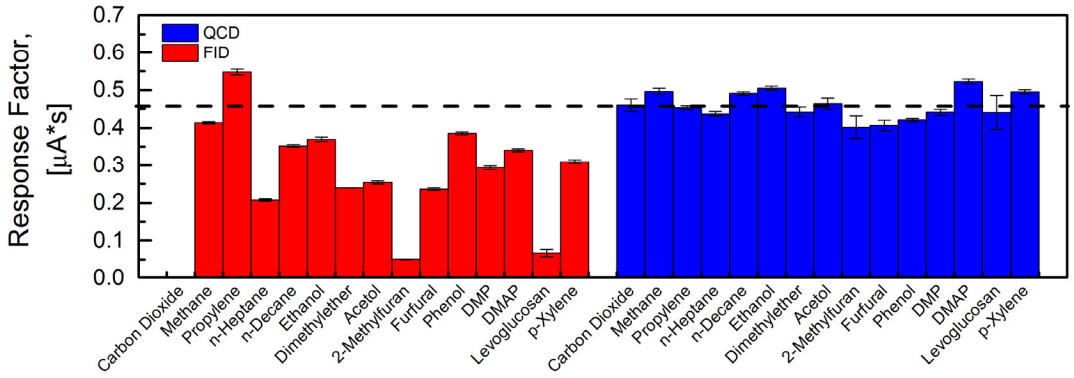

Figure 6. Response Factors of Conventional FID (Red) and QCD (Blue). Compound response factors (scaled using an internal standard of methane) analyzed using GC-FID vary over an order of magnitude, while response factors for compounds using GC-QCD are nearly constant within experimental error.

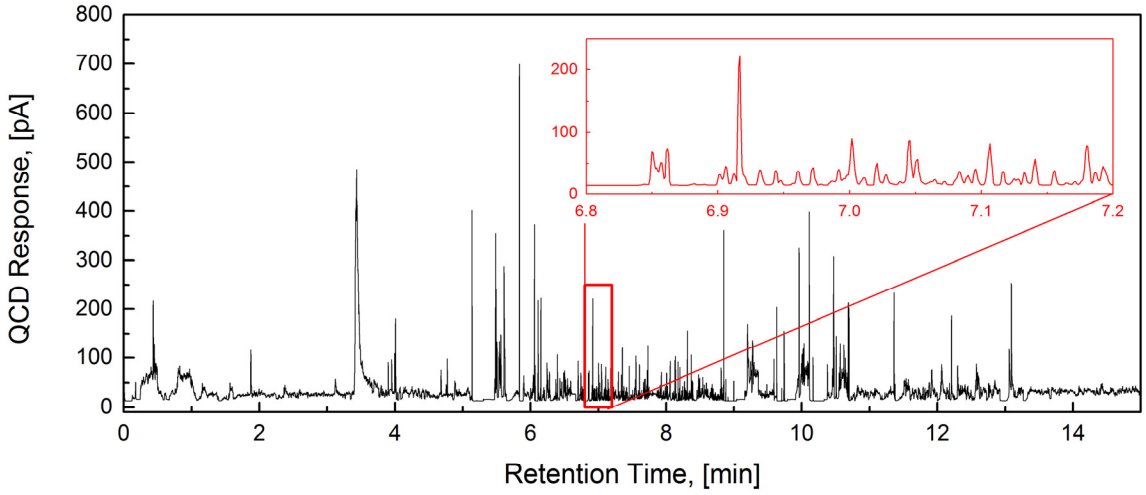

Figure 7. GC-QCD of Complex Mixtures Derived from Cellulose Pyrolysis. Chromatographic separation of products from ablative fast pyrolysis of microcrystalline cellulose at 500 °C was achieved for the complex mixture while maintaining peak resolution.

References

[1] A.V. Bridgwater, *J. Anal. Appl. Pyrolysis*, 1999, 51(1-2), 3-22.
[2] A. Oasmaa and D. Meier, *J. Anal. Appl. Pyrolysis*, 2005, 73(2), 323.
[3] H. Li, F. Jiku, and H.F. Schröder, *J. Chromatogr. A*, 2000, 889(1-2), 155-176
[4] T. Heberer, *Toxicol. Lett.*, 2002, 131, 5-17
[5] H. Van De Weghe, G. Vanermen, J. Gemoets, R. Lookman, and D. Bertels, "Application of comprehensive two-dimensional gas chromotography for the assessment of oil contaminated soils," *Journal of Chromatography A*2006, 1137, 1, 91-100
[6] A. M. Booth, P. A. Sutton, C. A. Lewis, A. C. Lewis, A. S. Scarlett, W. Chau, and S. J. Rowland, *Environ. Sci. Technol,* 2007, 41, 457-464
[7] A. F. Melbye, O. G. Brakstad, J. N. Kokstad, I. K. Gregersen, B. H. Hansen, A. M. Booth, S. J. Rowland, and K. E. Tollefsen, *Environ. Toxicol. Chem.*, 2009, 28, 9, 1815-1824
[8] B.M. Gordon, M.S. Uhrig, M.F. Borgerding, H.L. Chung, W.M. Coleman III, J.F. Elder, J.A. Giles, D.S. Moore, C.E. Rix, and E.L.White, *J. Chromatogr. Sci.*, 1988, 26(4), 174-180
[9] A.V. Bridgwater, D. Meier, and D. Radlein, *Org. Geochem.*, 1999, 30, 1479-1493.
[10] S. Kersten and M. Garcia-Perez, *Curr. Opin. Biotechnol.*, 2013, 24, 414.
[11] A. Oasmaa and D. Meier, *J. Anal. Appl. Pyrolysis*, 2005, 73(2), 323.
[12] A. Oasmaa and S. Czernik, *Energy Fuels*, 1999, 13, 914-921.
[13] P.M. Mortensen, J.D. Grunwaldt, P.A. Jensen, K.G. Knudsen, and A.D. Jensen, *Appl. Catal., A*, 2011, 407, 1-19.
[14] Paulsen, Alex D., Matthew S. Mettler, and Paul J. Dauenhauer. *Energy & Fuels* 27.4 (2013): 2126-2134.
[15] Mettler, M. S., Paulsen, A. D., Vlachos, D., & Dauenhauer, P. J., Catalysis Science & Technology, 2014, 10.1039/C4CY00676C
[16] Mettler, M. S., Paulsen, A. D., Vlachos, D. G., & Dauenhauer, P. J. *Energy & Environmental Science*, 2012, *5*(7), 7864-7868
[17] Mettler, M. S., Mushrif, S. H., Paulsen, A. D., Javadekar, A. D., Vlachos, D. G., & Dauenhauer, P. J., *Energy & Environmental Science*, 2012, *5*(1), 5414-5424.
[18] T. Watanabe, K. Kato, N. Matsumoto, and T. Maeda, *Chromatography*, 2006, 27(2), 49-55
[19] T. Watanabe, K. Kato, N. Matsumoto, and T. Maeda, *Talanta* 2007, 72, 1655-1658
[20] T. Watanabe, K. Kato, K. Tsunoda, and T. Maeda, *Anal. Chim. Acta*, 2008, 619, 26-29
[21] A.R. Teixeira, K.G. Mooney, J.S. Kruger, C.L. Williams, W.J. Suszynski, L.D. Schmidt, D.P. Schmidt, and P.J. Dauenhauer, *Energy Environ. Sci.*, 2011, 4, 4306.
[22] A. Sironi and G. Verga. U.S. Patent No. 5,373,725. 20 Dec. 1994.